Meteorol. Appl. 7, 1–18 (2000)

IR-based satellite and radar rainfall estimates of convective storms over northern Italy

R Amorati[1], P P Alberoni[2], V Levizzani[3] and S Nanni[4]

[1] *Institute FISBAT-CNR, via Gobetti 101, I-40129 Bologna, Italy and Dept. of Physics, University of Bologna, viale Berti Pichat 6/2, I-40127 Bologna, Italy*
[2] *ARPA-Servizio Meteorologico Regionale, Bologna, viale Silvani 6, I-40122 Bologna, Italy and Institute FISBAT-CNR, via Gobetti 101, I-40129 Bologna, Italy*
[3] *Institute FISBAT-CNR, via Gobetti 101, I-40129 Bologna, Italy and Visiting Scientist at EUMETSAT, Am Kavalleriesand 31, D-64295 Darmstadt, Germany*
[4] *ARPA-Servizio Meteorologico Regionale, Bologna, viale Silvani 6, I-40122 Bologna, Italy*

Convective precipitation events in northern Italy during 1996 and 1997 are analysed using two infrared-based geosynchronous satellite rainfall estimation methods to verify the level of applicability of the techniques for operational applications in the area, their quantitative results, and relative performances. The Negri–Adler–Wetzel (NAW) and the convective stratiform technique (CST) are applied to METEOSAT's thermal infrared (IR) data. C-band radar reflectivity fields detail the vertical and horizontal structure of the cloud systems, and radar rainfall data are retrieved. Satellite rain areas are checked against simultaneous radar rainfall retrievals through a contingency analysis procedure. A semi-quantitative analysis is presented. Positive brightness temperature differences between water vapour and thermal IR channels are also examined and related to the storms' development stage and rainrate. Results show that NAW and CST perform reasonably in delimiting rain areas during active convection and care should be used in the initial and final development stage when statistical parameters lose most of their significance. NAW tends to overestimate rainfall while CST approaches more closely radar measurements. Most common errors arise from considering only portions of the storm, contamination from cold non-precipitating cloud, and merging of two or more cloud masses of independent origin. Operational applications, though not completely quantitative, are also possible, including positive values of the difference between water vapour and IR brightness temperature.

1. Introduction

Satellite rainfall estimations using thermal infrared (IR) data from geosynchronous satellites have been used for nearly three decades. The great majority were initially developed for convective systems (Gruber, 1973), specially those in the tropics, and application ranges from the climatological down to the instantaneous rainrate scale. The GOES Precipitation Index (GPI) (Arkin, 1979; Arkin & Meisner, 1987) is a standard for climatological rainfall analysis regularly applied over tropical areas. The relatively straightforward satellite detection of tropical convective cloud systems and the possibility of separating cumulonimbus towers from the stratiform anvil was effectively used in several methods. Among others we recall the Griffith-Woodley technique (Griffith *et al.*, 1978), the Negri–Adler–Wetzel technique (NAW) (Negri *et al.*, 1984), and the convective stratiform technique (CST) (Adler & Negri, 1988). Thresholding methods were also applied to produce rain estimations for periods of ten days or more: see, for example, the application to the River Nile catchment by Todd *et al.* (1995).

Several authors used the combination of satellite IR and visible (VIS) channels at mid-latitudes. Bellon *et al.* (1980) included VIS data in their RAINSAT technique for screening out cold but not highly reflective cloud tops to reduce false alarms induced by IR techniques. Tsonis & Isaac (1987) classified pixel clusters in the VIS/IR histogram of the cloud scene and assigned rainfall amount. All these methods are trained or calibrated using radar data either from single radar (Bellon *et al.*, 1980) or a network, as recently done in the UK by Cheng & Brown (1995).

Barrett & Martin (1981) and Kidder & Vonder Haar (1995) provide excellent reviews of satellite rainfall estimation methods in their books. Petty (1995) concentrated on estimations over land and Levizzani (1998) on geosynchronous satellite data.

The importance of satellite monitoring for extreme precipitation events has become evident in recent times when satellite techniques were applied to heavy rain monitoring for disaster risk management. Barrett & Michell (1991) give a clear idea of the problem in the Mediterranean basin. Flash flood monitoring in the US, a crucial issue for the national weather prediction system, is becoming operational (Scofield & Naimeng, 1994; Vicente & Scofield, 1996; Vicente *et al.*, 1998). Applications to Italy's precipitation systems have been attempted on several occasions over various time scales and for different precipitation systems. Levizzani *et al.* (1990) explored the limitations of IR techniques for frontal rain detection over the Arno River basin. Squall-line and frontal storm rain-inducing floods were also examined by Levizzani *et al.* (1996). Marrocu *et al.* (1993) estimated rain amount over Sardinia, and Pompei *et al.* (1995) attempted a validation against the regional raingauge network. Porcù *et al.* (1996, 1998) analysed stratiform rain from a hydrological perspective.

Satellite IR rain estimation, though far from being quantitatively satisfactory, is still of great interest for the potential nowcasting application together with radar observations. Convective storms in the Po Valley of northern Italy have been studied already in the 1970s using radar reflectivity, and mesoscale and microphysical analyses (Prodi & Wirth, 1973; Prodi, 1974). More recently mesoscale analysis, numerical modelling and Doppler radar studies were conducted on severe thunderstorm outbreaks (Alberoni *et al.*, 1993, 1996). However a climatological study by Cacciamani *et al.* (1995) points out that there is insufficient knowledge of the Po Valley storms for their effective forecast. The authors suggest the need for observations from non-conventional meteorological platforms for the determination of storm structures and their relationships with synoptic and mesoscale weather systems. Frontal passages in particular and the interactions with the Alpine range have demonstrated to be the most important triggering mechanism of severe thunderstorm development in the area (Buzzi & Alberoni, 1992; Alberoni *et al.*, 1998; Levizzani *et al.*, 1998).

NAW and CST techniques were applied to spring/summer storms and frontal embedded convection, and the results analysed against radar rainfall retrievals. Early results of the analysis can be found in Levizzani *et al.* (1997). A mesoscale framework of each storm is given in section 2. Satellite techniques, radar data and rainfall retrievals are described in some detail in section 3. The contingency analysis and semi-quantitative considerations are provided using radar to define two rain categories (heavy and light rain): results are presented in sections 4 and 5. A discussion on the role of water vapour (WV) and IR positive brightness temperature differences above deep convection in METEOSAT imagery is the object of section 6. Sections 7 and 8 present a discussion, conclusions and suggestions for future studies.

2. Convective episodes

Five convective episodes during 1996 and 1997 were examined to document different storm types and evolution from single cell to supercell, with a case of convection embedded in a frontal system.

On 8 August 1996 a fast moving wave approached Italy from the west. Figure 1 shows the geopotential and temperature fields at 500 hPa at 0000 and 1200 UTC. At 0000 UTC the wave was located over the Iberian peninsula and well pronounced at medium levels, with a co-located minimum in the temperature field. A frontal system was located north of the Alps, and the instability induced by the wave depression triggered a late morning and afternoon thunderstorm formation over the Po Valley. At noon the fast moving wave approached the Italian coast and a baroclinic area ahead of the wave fed the convection (Figure 1(*b*)). During the next few hours the system travelled over central Italy, and at 0000 UTC on the next day weakened aloft

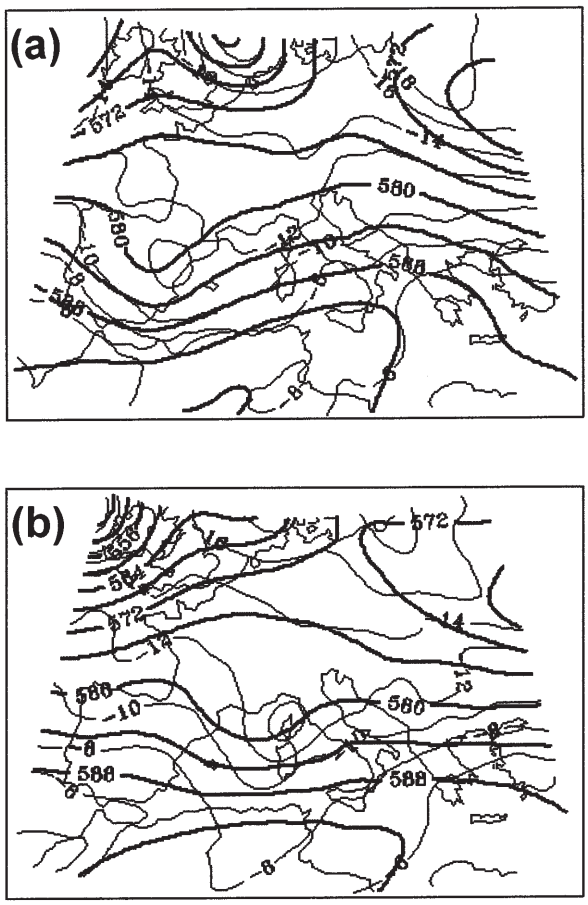

Figure 1. *Geopotential height (thick) and temperature fields (thin) at 500 hPa for* (a) *0000 UTC and* (b) *1200 UTC on 8 August 1996. Geopotential height units are dam and temperature units are °C.*

and disappeared at the ground with only a residual weak temperature gradient over the Dinaric Alps.

On 31 August 1996 severe convection phenomena occurred during the first half of the day. The synoptic situation at 500 hPa was characterised by a deep trough centred over northern Europe, while at lower levels a persistent geopotential low was centred over Italy. Maps in Figure 2 refer to the end of the most active period when the system was ready to leave northern Italy. At 0000 UTC the baroclinic perturbation approached the Tyrrhenian coast: the 850 hPa geopotential field was characterised by a closed low. Six hours later the geopotential low had deepened and the incoming baroclinic area was over the Po Valley. At the same time convection had started owing to the frontal passage. During the rest of the day the frontal displacement and the end of the convection accompanied a less pronounced perturbation at higher levels over northern Italy.

Severe weather on 2 October 1996 was characterised by convection embedded in a frontal system, which is typical for the Mediterranean during fall when the Azores anticyclone weakens and the polar front moves southwards with large depressions at low levels and troughs at medium–high levels. The instability triggered by such passages is substantial, and mesoscale convective systems often arise and cause extensive precipitation and flood hazard. In the present case there was a trough at 850 hPa on 1 October over western Europe together with a front associated with a strong temperature gradient. At 0000 UTC on 2 October the trough had reached the Mediterranean Sea and the front was split in two by the orography, the first part centred over central Europe while the other part swept across the Mediterranean from Sardinia to Africa (Figure 3(*a*)). Upper-level charts (not shown) exhibit a deep trough not disturbed by the Alps, and frontal high-level cloudiness was advected over northern Italy. When these types of synoptic features occur a secondary cyclone develops most of the time south of the Alps. During the next twelve hours a geopotential minimum at 850 hPa developed and deepened while the storms had already started forming since the early morning in the western Po Valley reaching the area covered by the radar around midday. At noon (Figure 3(*b*)) the low at 850 hPa was fully developed and centred over northern Italy. It drove a re-circulation of moist air from the Adriatic Sea impinging over the southern slope of the Alps, inducing heavy rainfall. At upper levels the meteorology was characterised by the displacement of the trough over Italy and further development of a cut-off low moving south.

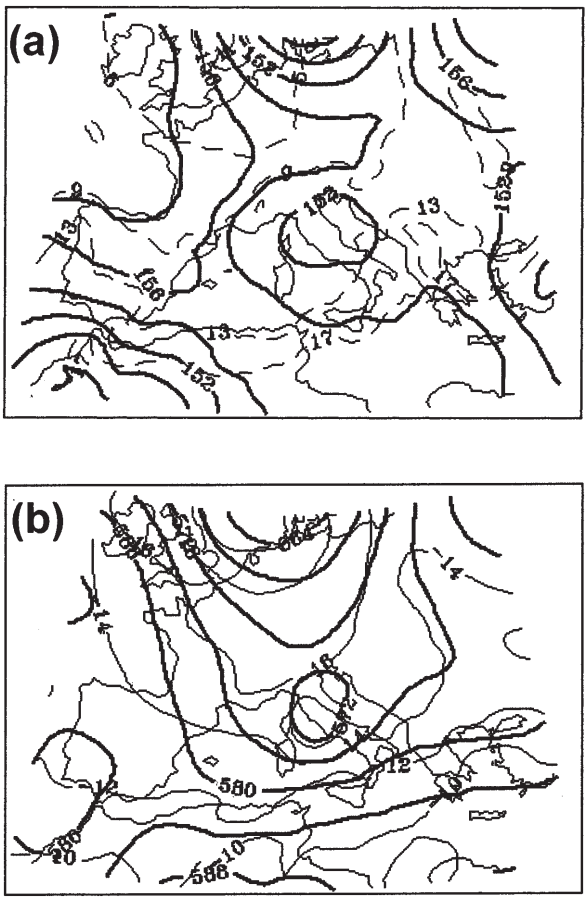

Figure 2. *As Figure 1 but for* (a) *850 hPa and* (b) *500 hPa at 1200 UTC on 31 August 1996.*

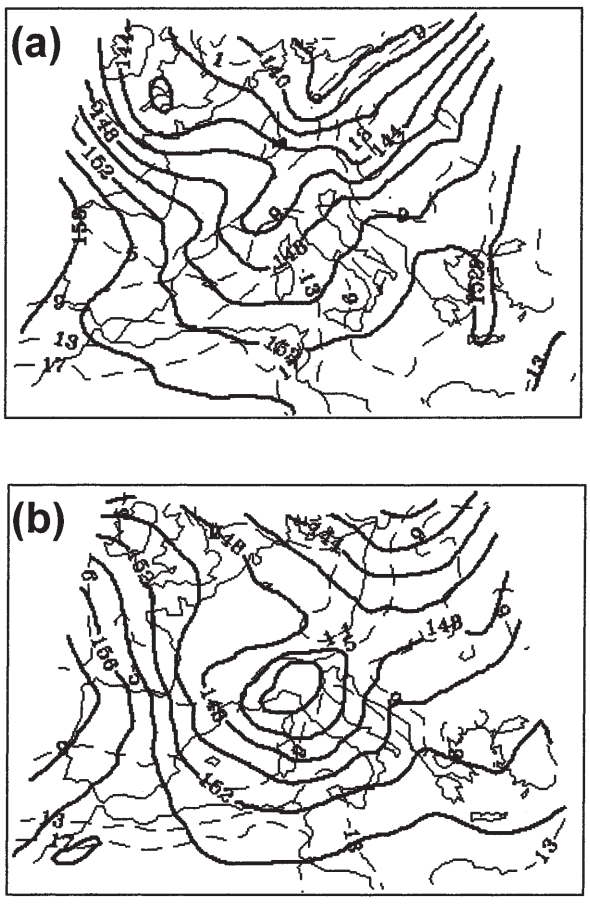

Figure 3. *As Figure 1 but for 850 hPa at* (a) *0000 UTC and* (b) *1200 UTC on 2 October 1996.*

30 April 1997 was dominated by a post-frontal convective activity (Figure 4). At 0000 UTC an occluded cyclone was positioned above southern Italy. The system slowly moved south-east at 850 hPa crossing the Ionian Sea and reached the spine of the Peloponnese in southern Greece at 0000 UTC on 1 May. At 500 hPa the depression progressively enlarged from 0000 UTC on 30 April to cover the whole of southern Italy by 1200 UTC, gradually separating from a corresponding weakening low-pressure area over northern European countries. Moist air advected from the east by the cyclonic circulation increased the local instability above the Po Valley. Short-living storms with significant electric activity and hailfall were generated at the centre of the Valley and travelled south advected by high-level winds.

The most severe convective episode considered in this study occurred on 18 June 1997, when two simultaneous supercells formed in the Po Valley, yielding damaging hailfalls (Alberoni *et al.*, 1998). The synoptic situation was characterised by a cut-off low at 500 hPa located over the Iberian Peninsula, which is visible in Figure 5. At 0000 UTC the high-level geopotential field over Italy showed a strong south-west flow. A short baroclinic wave superimposed on this large-scale structure and positioned over central Europe travelled south-east. The temperature gradient at 500 hPa identifies the position of the front at this time (Figure 5(*a*)). At 850 hPa (not shown) the thermal pattern reveals the presence of two separated fronts, the first over the Alps and the other extending from north Africa to central Italy. The geopotential field shows a less-defined trough over Europe and a local high south of Sicily that enforced the warm moist advection from the Mediterranean Sea. Twelve hours later (Figure 5(*b*)) the 500 hPa cut-off low had moved south-west with a more pronounced zonal flow over Italy, the most important feature being the fast displacement and rapid growth of the baroclinic disturbance over central Europe. At this time the short wave had reached the Alpine chain. The warm advection is clearly visible in the temperature field from the displacement over Sardinia of the –12 °C isotherm (more than 400 km in 12 hours).

3. Data processing

3.1. Satellite rainfall estimations

Two different methods were used to estimate rainfall from thermal IR METEOSAT data: the Negri–Adler–Wetzel technique (Negri *et al.*, 1984) and the convec-

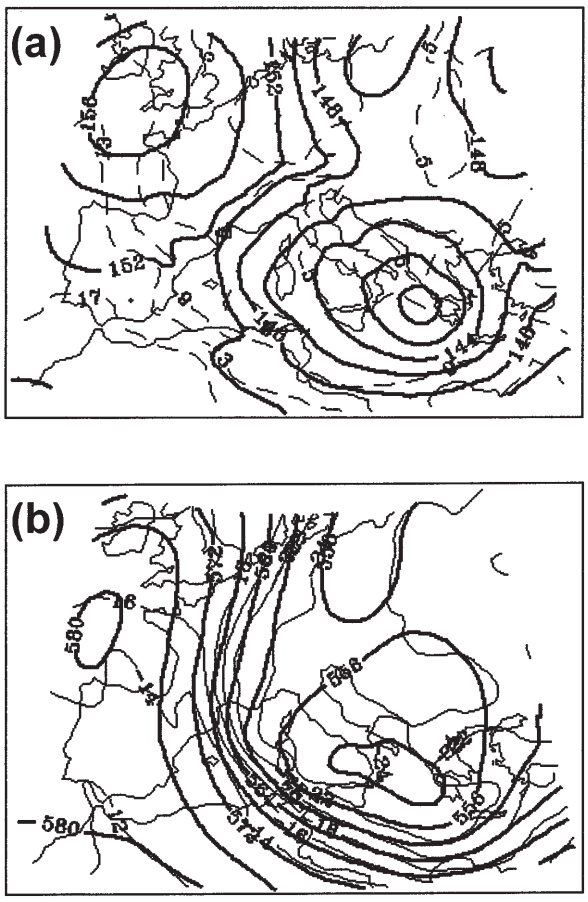

Figure 4. *As Figure 1 but for* (a) *850 hPa and* (b) *500 hPa at 1200 UTC on 30 April 1997.*

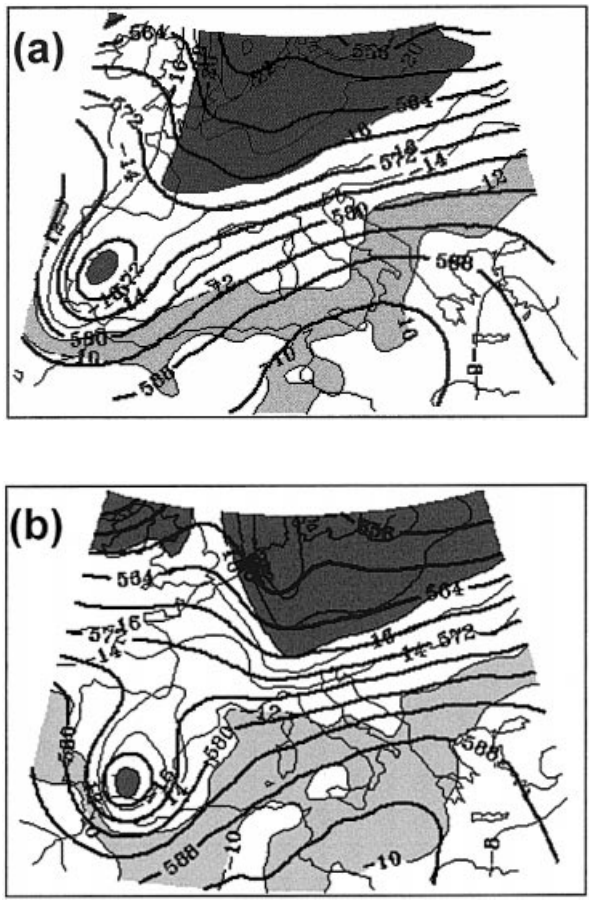

Figure 5. *As Figure 1 but for 500 hPa at* (a) *0000 UTC and* (b) *1200 UTC on 18 June 1997. Light grey shades refer to temperatures between -10 and -12 °C and dark grey shades to temperatures below -18 °C.*

tive stratiform technique (Adler & Negri, 1988), referred to as NAW and CST, respectively. Both algorithms were originally developed for tropical cumulonimbus clouds over the ocean off the coast of Florida and since then widely used to examine tropical and extra-tropical meteorological situations (e.g. Levizzani *et al.*, 1990, 1996; Negri & Adler, 1993; Bendix, 1997).

The NAW technique represents an evolution of the Griffith–Woodley technique (GW), a life-history-type scheme by Griffith *et al.* (1978) based on combined satellite and radar observations (details on life-history methods are given by Barrett & Martin, 1981). The NAW simplifies the GW method by introducing a computationally efficient procedure entirely based on geostationary satellite IR imagery. Its application to mid-latitude precipitation systems is by no means without difficulty. Using METEOSAT's IR imagery, Levizzani *et al.* (1990), Marrocu *et al.* (1993) and Pompei *et al.* (1995) reported that the best performance of the NAW at mid-latitudes is obtained for rainfall estimates averaged over suitable space-time intervals. However, their findings were based on a comparison with raingauge networks: radar data were needed for a more thorough investigation. Porcù *et al.* (1996) used radar rainfall retrievals and reached the same conclusions while focusing on frontal heavy precipitation.

In the original NAW algorithm conceived for the Florida Area Cumulus Experiment (FACE), the cloud area (A_C) was identified by the 253 K isotherm, with isotherms $T_{50\%}$ and $T_{10\%}$ defining the 50% and 10% coldest portions of the cloud area, respectively. Assuming the rain volume R_V is directly proportional to A_C, three brightness temperature (T_B) thresholds were chosen for the rainrate (RR) assignment during FACE. RR = 8 mm h^{-1} for $T_B < T_{10\%}$ (heavy rain, HR), RR = 2 mm h^{-1} for $T_{10\%} < T_B < T_{50\%}$ (light rain, LR), and RR = 0 for $T_B > T_{50\%}$. These rainrate values are independent of the cloud life history and calibrated using convective rainfall from decaying cumulonimbus over Florida with lifetimes of 1 to 3 hours. Rainrate assignments and temperature thresholds can be varied according to intrinsic thermodynamic stability, background cloud condensation nuclei concentrations, topography, terrain height, and the general nature of the local synoptic flow regimes. For the present study, the NAW algorithm was applied in the version of Levizzani *et al.* (1996).

The convective stratiform technique was conceived for the discrimination of convective from stratiform rain for tropical cumulonimbus clouds. Rainfall is estimated on an image-by-image basis, as it is for NAW. First, pixels associated with temperature levels higher than 253 K are rejected on the IR image and temperature minima T_{min} subsequently located. A slope parameter is calculated in order to distinguish convective cores from non-precipitating cirrus. The slope is a measure of the gradient about the minimum point. Minima with slope greater than a linear discriminant function are supposed to be convective cores, while minima with smaller slope parameters are classified as cirrus. Rainrate and convective rain area are computed as an empirical function of T_{min}. Starting from the location of the minimum, rainrate is assigned to the closest pixels until the computed area is covered. The stratiform precipitation is assigned using a temperature threshold T_s which defines the mature anvil region. A test is applied to identify mature thunderstorm stages: only minima with slope smaller than an empirical value (provided they passed the cirrus test) are considered embedded in a region of precipitating anvils and used to compute the stratiform threshold. T_s is the weighted mean of mode temperatures counted for every convective cloud. A rainrate of 2 mm h^{-1} is assigned to pixels associated with temperatures lower than the stratiform threshold.

NAW and CST were applied to the five convective episodes described in section 2. Half-hourly METEOSAT-5/6 IR images in the 10.5–12.5 μm thermal IR window channel were used with a ground resolution of about 6 × 8 km^2 over the examined area. The 5.7–7.1 μm WV channel was also used. During the night images in this spectral band were transmitted from METEOSAT at half-hourly intervals, while from 0600 UTC to 2000 UTC (slot 12 to slot 40), when high-resolution visible images were available, the dissemination time was hourly. The ground resolution for WV is the same as for the IR channel. For every episode, an area including the radar coverage and the whole cloud system was extracted and processed. The inclusion of the totality of a cloud system is of fundamental importance for the correct apportionment of the cold cloud top areas by the two techniques: if a significant portion of the cloud is cut out of the image, the rain assignment can be significantly different.

3.2. Radar data

Rainfall estimates used as 'ground truth' were retrieved from volume scans of the C-band Doppler weather radar of the Regional Meteorological Service located 20 km north-east of Bologna in San Pietro Capofiume. Reflectivity data were recorded every 15 minutes with a lobe of 0.9° and radial resolution of 250 m. Data were pre-processed as follows.

(a) First, a dynamic clutter suppression algorithm was run over raw data by the radar pre-processor. The filter is based on an infinite impulse response (IIR) implementation of the three-pole elliptic filter proposed by Groginski & Glover (1980).
(b) A clutter and anomalous propagation cancellation algorithm (Alberoni & Nanni, 1996; Andersson *et al.*, 1997) was then run over the integrated data to remove any residual spurious echoes not cancelled by the Doppler filter.

(c) Finally, reflectivity data were converted into rainfall intensity using the standard Marshall & Palmer (1948) relationship and reported on a regular 1 km resolution Cartesian grid and a total coverage of 250×250 km^2 centred on the radar site.

In order to compare satellite rainfall estimates with ground truth the radar rainrate was re-mapped onto the METEOSAT grid. The high-resolution radar field (1×1 km^2) was degraded and adapted to the satellite resolution (6×8 km^2). Every satellite pixel not filled by radar observations was rejected from the analysis. Figure 6 shows the radar coverage with the overlapped satellite grid. METEOSAT scans northern Italy at the 21st and 51st minute every hour, while the radar scans were available every 15 minutes, starting at the full hour. The time lag between radar observations and the closest satellite images was therefore of about 6 minutes.

4. Contingency analysis of the results

A pixel-by-pixel analysis was conducted to verify the delineation of the rain area by the satellite techniques. Table 1 shows the contingency table constructed for NAW and CST. Such a table is normally used to check model output results against an independent 'truth', a typical example being numerical weather forecast scores. In this case the satellite rain estimate is considered the model output and the radar retrieval the 'ground truth'.

A scalar measure of the accordance between the rain area estimated by the satellite and the one observed by the radar can be quantitatively expressed by the following statistical parameters derived from quantities in Table 1 (Wilks, 1995):

$$CSI = \frac{d}{c + b + d}$$

$$FAR = \frac{c}{c + d}$$

The *critical success index* (*CSI*) is the fraction of correctly estimated rainy pixels with respect to those either observed (radar) or estimated (satellite); the *false alarm ratio* (*FAR*) is the fraction of pixels estimated rainy by the satellite which in fact were observed non-rainy by the radar. For a perfect satellite estimate *CSI* and *FAR* take the value 1 and 0, respectively, while for a completely incorrect estimate *CSI* is 0 and *FAR* is 1. The intrinsic statistical nature of both parameters makes them lose their significance when too few rainy pixels are present. Note that the results of the contingency analysis are by no means unequivocal in this respect and depend on the total number of rainy pixels, as will be shown in the following.

Table 1. *Contingency table for the satellite-radar comparative analysis. Satellite estimates are considered model output to be checked against radar retrievals treated as 'ground truth'.*

Estimated (satellite)	Observed (radar)	
	No rain	Rain
No rain	a	b
Rain	c	d

CSI and *FAR* curves for NAW and CST for the five events are presented in Figure 7. On 8 August 1996 the *CSI* behaviour is very similar for both techniques in the first part of the event, reaching a maximum of about 0.7 at 1621 UTC, and thereafter NAW is associated with better values. *FAR* has the same behaviour for both techniques except from 1651 to 1851 UTC, when for CST it reaches values very close to 0. The number of rainy pixels either observed by radar or estimated by CST and NAW for all events is presented in Figure 8, together with the mean rainrate values. For the CST the mean rainrate has been restricted to the central part of the events, since at the very beginning and the very end of convection too few pixels survive the selection criteria, inducing unreasonable values. CST underestimates the rainy pixels during the last phase of the storm, while NAW constantly overestimates them. The CST underestimation implies a lower probability of detecting rainy pixels and consequently a decrease in the number of false alarms. CST shows a peak at 1151 UTC, which is much higher than the radar retrieval. Afterwards the technique computes values much closer to those from the radar, and the curve closely follows the corresponding one from the radar until 1621 UTC, the time of the absolute maximum of the number of rainy pixels.

On 31 August 1996 NAW's *CSI* is higher than that of CST for the whole event. *FAR* is consistently smaller for CST at all times. A maximum *CSI* of about 0.8 at 1251 UTC for the NAW and 0.6 at 0851 UTC for the CST correspond to local *FAR* minima, revealing an accordance of satellite and radar in the assignment of rain area and rainy pixel spatial distribution. CST always assigns a smaller number of rainy pixels with respect to radar while NAW overestimates. The gap between the two techniques widens during the final part of the storm as in the previous case. The satellite estimates drop to zero before 1521 UTC, while the radar continues detecting light rain for several hours. This is because rain is no longer convective and the techniques are unable to delineate cold rainy clouds from the IR. The unreasonably high *FAR* values after 1451 UTC are consistent with the end of the convective activity.

The different meteorological framework of 2 October 1996 (see section 2) reflects on the application of CST.

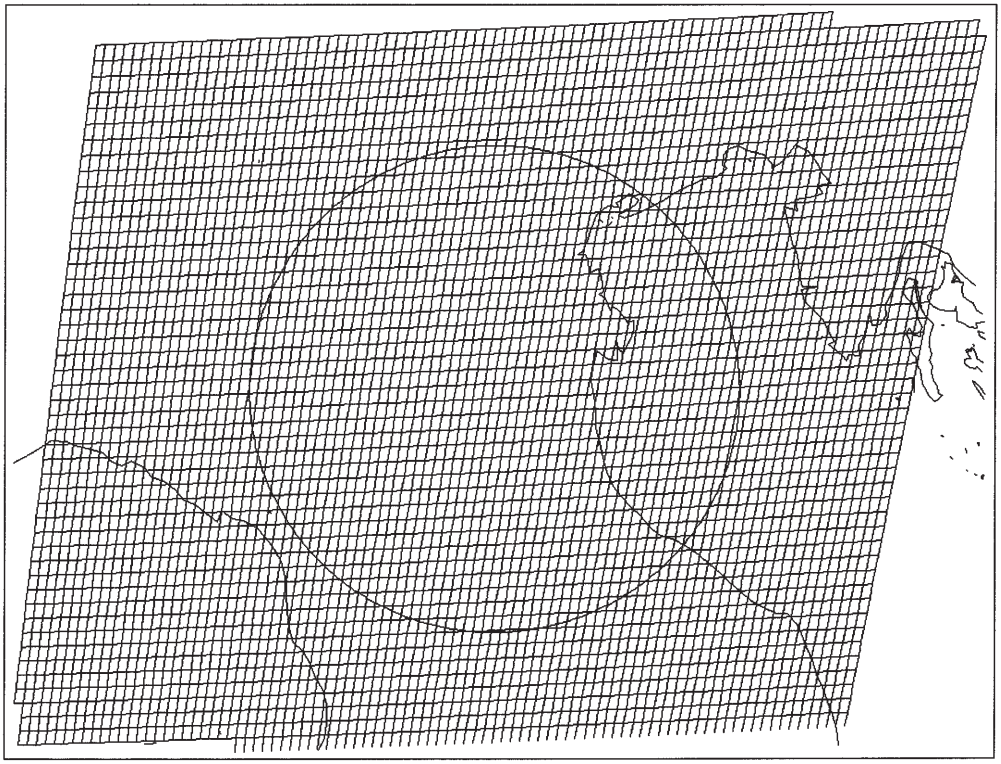

Figure 6. *Area of the case studies with radar coverage and projection of the METEOSAT pixels.*

The event is mainly stratiform and the CST output is clearly inconsistent. *CSI* and the total number of rainy pixels show a rather jagged behaviour, a clear symptom of the lack of applicability of the technique. The NAW output is much more regular, though a significant overestimation is detected all the way up to 0951 UTC (see Figure 8). The very high *FAR* values in Figure 7 together with the low number of rainy pixels as detected by the radar (Figure 8) indicate the presence of high-level cloudiness in the first part of the day during the approach of the front. NAW considers these high cold clouds as precipitating, thus completely missing the nature of the event. After 0951 UTC a series of small thunderstorms formed, and this was detected by the radar. NAW performs reasonably, only slightly overestimating the anvil rainfall.

On 30 April 1997 *CSI* and *FAR* show comparable values for the two techniques throughout the greatest part of the storm. The maximum value of *CSI* is much lower than those registered in the previous cases. The number of pixels wrongly assigned precipitation by the satellite is of the same order of magnitude as for the other cases, but their relative weight is much higher since it was an isolated short-living storm.

Cirrus clouds induced a strong overestimation by NAW on 18 June 1997 before 1200 UTC. NAW and CST exhibit matching values of both *CSI* and *FAR*. In the middle of the development of the twin supercells described in section 2 both satellite techniques show a peak in the number of rainy pixels corresponding to a radar maximum. At the end of the event the CST rainrate does not dramatically reduce prior to NAW and radar, unlike what happened in the previous cases. A possible explanation is that the storms were still very much convectively active when they left the area covered by the radar beam.

In all five cases the best *CSI* and *FAR* values for NAW and CST are attained during the central phase of the event when convection and precipitation are more intense and the delineation of the rainy area is more efficient. When too few pixels are assigned precipitation, the statistics no longer become applicable to satellite rain detection. For all the events both techniques satisfactorily delimit rain areas though NAW performs better rain/no-rain detection despite its computational and conceptual simplicity. Problems arise in the presence of cirrus clouds, as noted for the 2 October 1996 and 18 June 1997 events, and this is particularly true for NAW. CST's overestimation of rainy pixels is generally lower than that of NAW even if the cirrus test does not completely eliminate non-precipitating clouds. The decrease of rainy pixel number as estimated by the CST happens before that of NAW towards the end of the events. Mean rainrate values from satellite agree reasonably well and the overall trend matches that from radar. For the most part the satellite techniques overestimate radar mean rainrates by a few mm h^{-1} as expected. An interesting feature is shown in the radar mean rainrate on 18 June 1997 during the development of the supercells: the jaggy trend seems to refer to short-period convective showers.

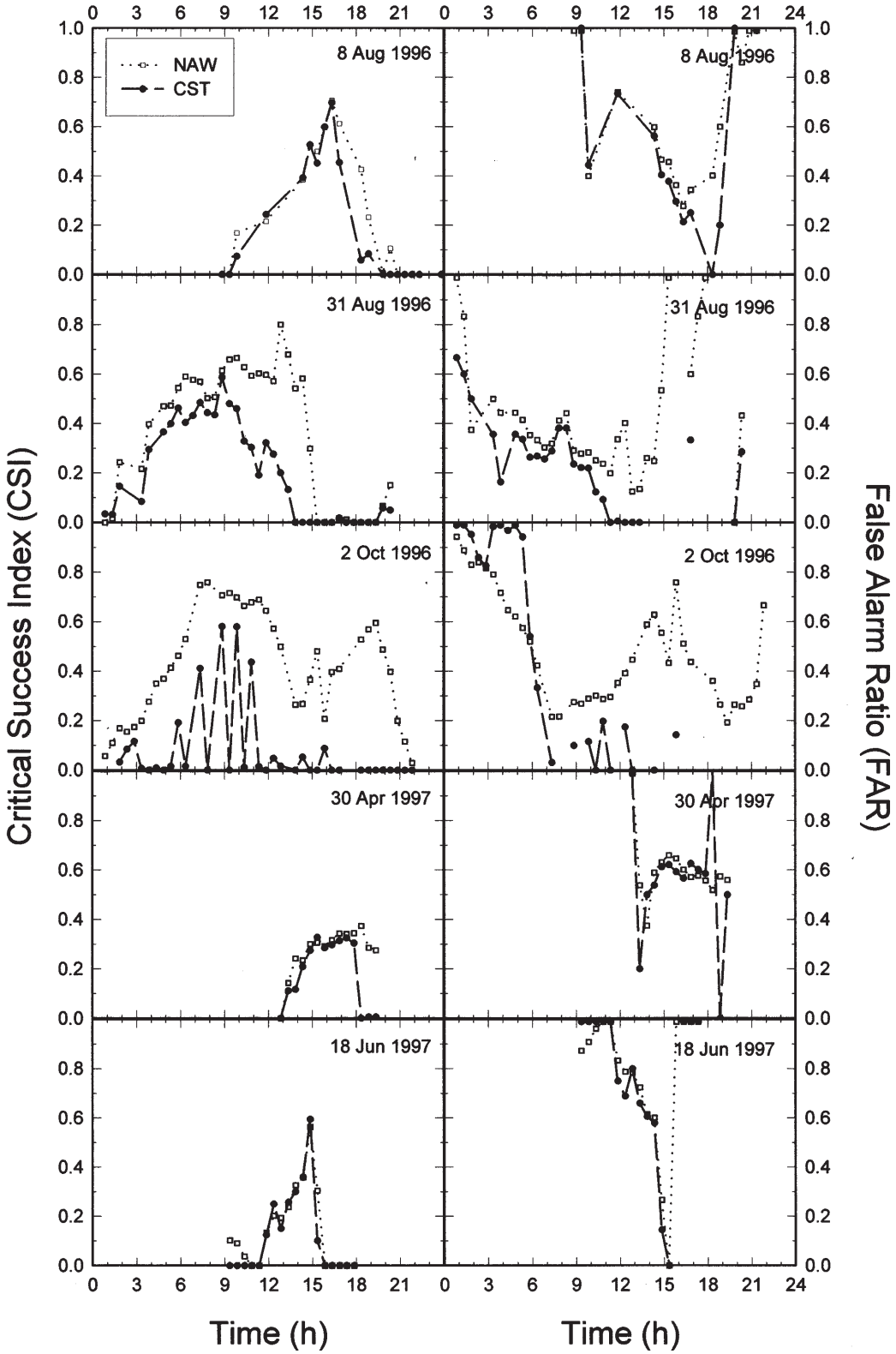

Figure 7. *CSI (left) and FAR (right) for NAW (dotted and hollow square) and CST (dashed and filled circle).*

5. Quantitative analysis of the results

Two measures of the agreement of satellite estimates and radar observations were adopted: the bias and the root mean square difference (rmsd). They are defined as follows:

$$bias = \mathrm{E}[(Y_i - O_i)]$$

$$rmsd = \sqrt{\mathrm{E}[(Y_i - O_i)^2]}$$

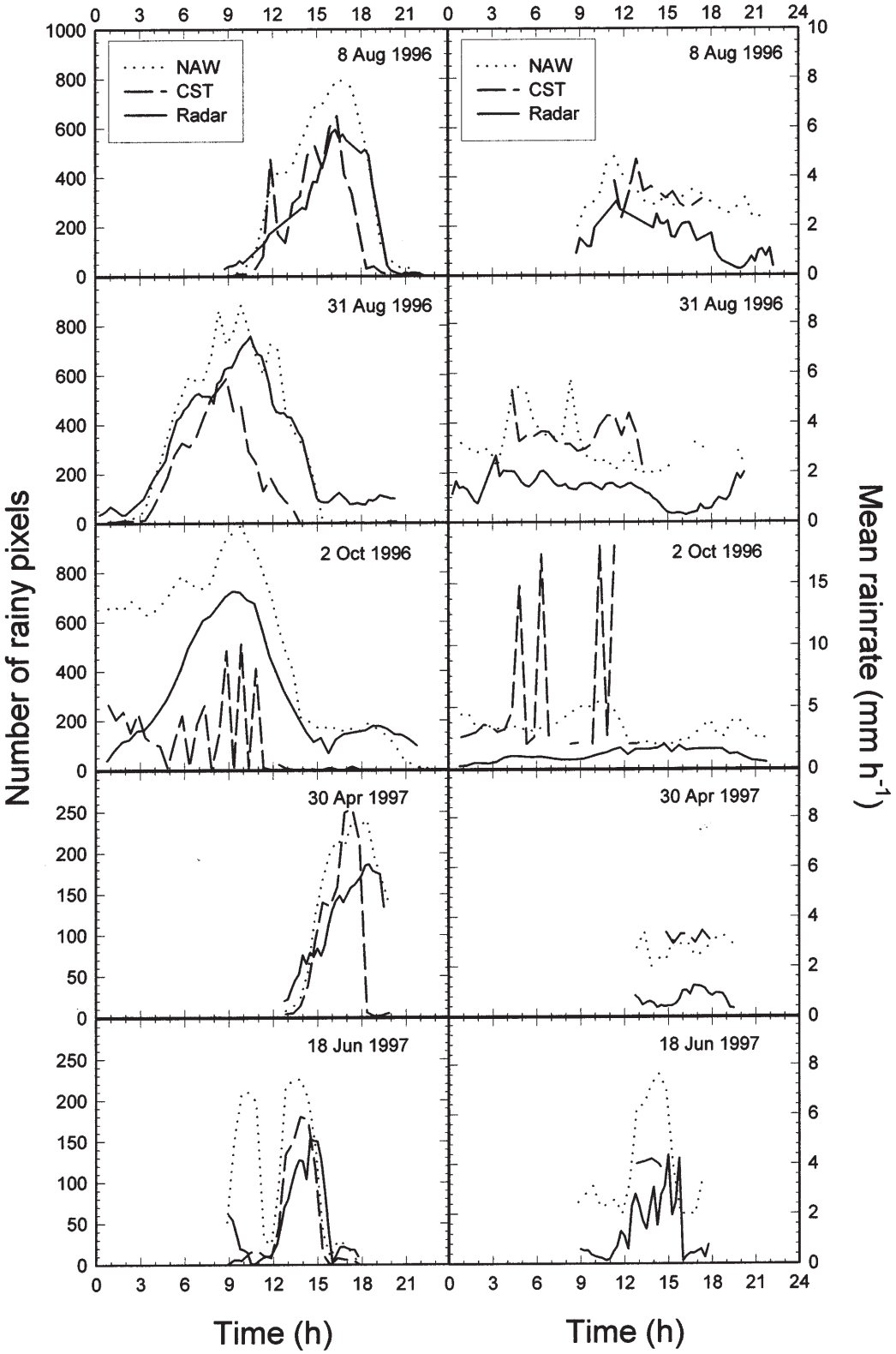

Figure 8. *Number of rainy pixels over the radar coverage (left) and mean rainrate (right) as estimated by NAW (dotted) and CST (dashed), and retrieved by radar (solid).*

where Y_i is the satellite-estimated rainrate over the ith pixel, O_i is the correspondent radar observation, and $E[\ ]$ is the expected value or mean. Both parameters were computed excluding all 'trivial' pixels where both radar and satellite detected no rain.

As a first step the original calibrations of NAW (Negri *et al.*, 1984) and CST (Adler & Negri, 1988) were adopted. In Figure 9 the total rainrate estimated by the two satellite techniques and observed by radar is shown; the associated bias and rmsd are shown in Figure 10. Three peaks characterise NAW and CST

rainfall estimations on 8 August 1996. CST's rainrate is generally lower and closer to radar observations. A slight underestimation characterises the final part of the event, as expected from the previous analysis of the decrease of number of rainy pixels. NAW constantly overestimates during the entire event. The bias is in fact positive in the central part of the event for NAW with a maximum value of 2.4 mm h^{-1} (mean rainrate 4.2 mm h^{-1}), while for CST it reaches a peak of 1.8 mm h^{-1} (mean rainrate 3.4 mm h^{-1}). CST's rmsd is higher than NAW's in the central part of the event, an index of the relatively large difference between CST and radar at this time. This implies that the smaller bias is not an absolute guarantee that CST performs better than NAW on a pixel-by-pixel basis. The two peaks in CST's bias at 1951 and 2121 UTC are an artefact of the statistics, given the very low number of pixels at this stage. This happens frequently at the very beginning and towards the end of the storms, causing the statistics to lose its validity, as will be shown in the following cases.

NAW and CST total rainrate curves on 31 August 1996 show a similar shape, with CST systematically below NAW. Bias is lower for CST (max 1.2 mm h^{-1}, mean rainrate 3.1 mm h^{-1}) than for NAW (max 4.4 mm h^{-1}, mean rainrate 5.8 mm h^{-1}), and rmsd is similar. The same considerations on bias and rmsd apply to spurious peaks at the beginning and the end of the storm as well as to low values of the bias, as in the previous case. A peak of rainrate at 0821 UTC rises very much above the background of the NAW analysis and the same happens for bias and rmsd. A close examination of the IR field reveals that two cloud systems travel: one across the radar coverage and the other south of it at this time of the day. The northernmost is the convective system under examination and the southern one belongs to the frontal zone extending from north Africa to southern Italy (see Figure 2). The two cloud systems are well separated in the IR imagery at 0751 and 0851 UTC, while they appear somehow connected at 0821 UTC. This strongly influences the attribution of the cold cloud area as done by NAW. In other words at 0821 UTC NAW considers the two cloud masses as one, and the result is a significant overestimation of the amount of pixels belonging to the 10% coldest cloud portion. The same happens for the smaller peak between 1151 and 1221 UTC. The relative importance of the two peaks is correlated to the presence of active convective cells on the vertical of the radar. In the first case the most active part of the system was located above the radar site, and this led to an excessive overestimation by the NAW; in the second case convection had moved away from the radar coverage, and more stratiform rain was detected.

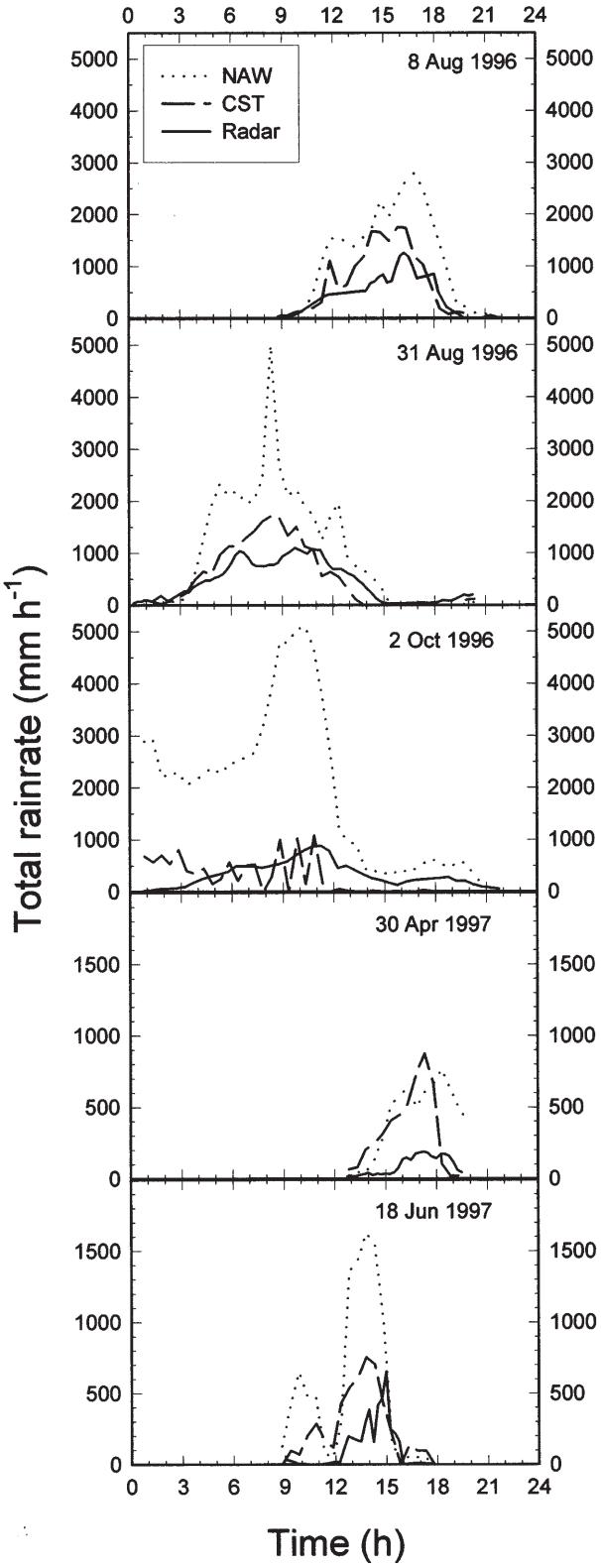

Figure 9. *Total rainrate in mm h^{-1} over the radar coverage as estimated by NAW (dotted) and CST (dashed), and retrieved by radar (solid).*

NAW precipitation on 2 October 1996 is largely overestimated and this is particularly true in the first half of the day. The cloud system was frontal and extended over a very large area so that NAW identifies a huge 'precipitating' cloud. There are, though, no local temperature minima that uniquely identify the single storm, since the convection was embedded in the frontal system. The bias reaches the maximum value of about 4.4 mm h^{-1} and rmsd of 5.4 mm h^{-1} (mean rainrate 5.1 mm h^{-1}). Note once more the persistent instability

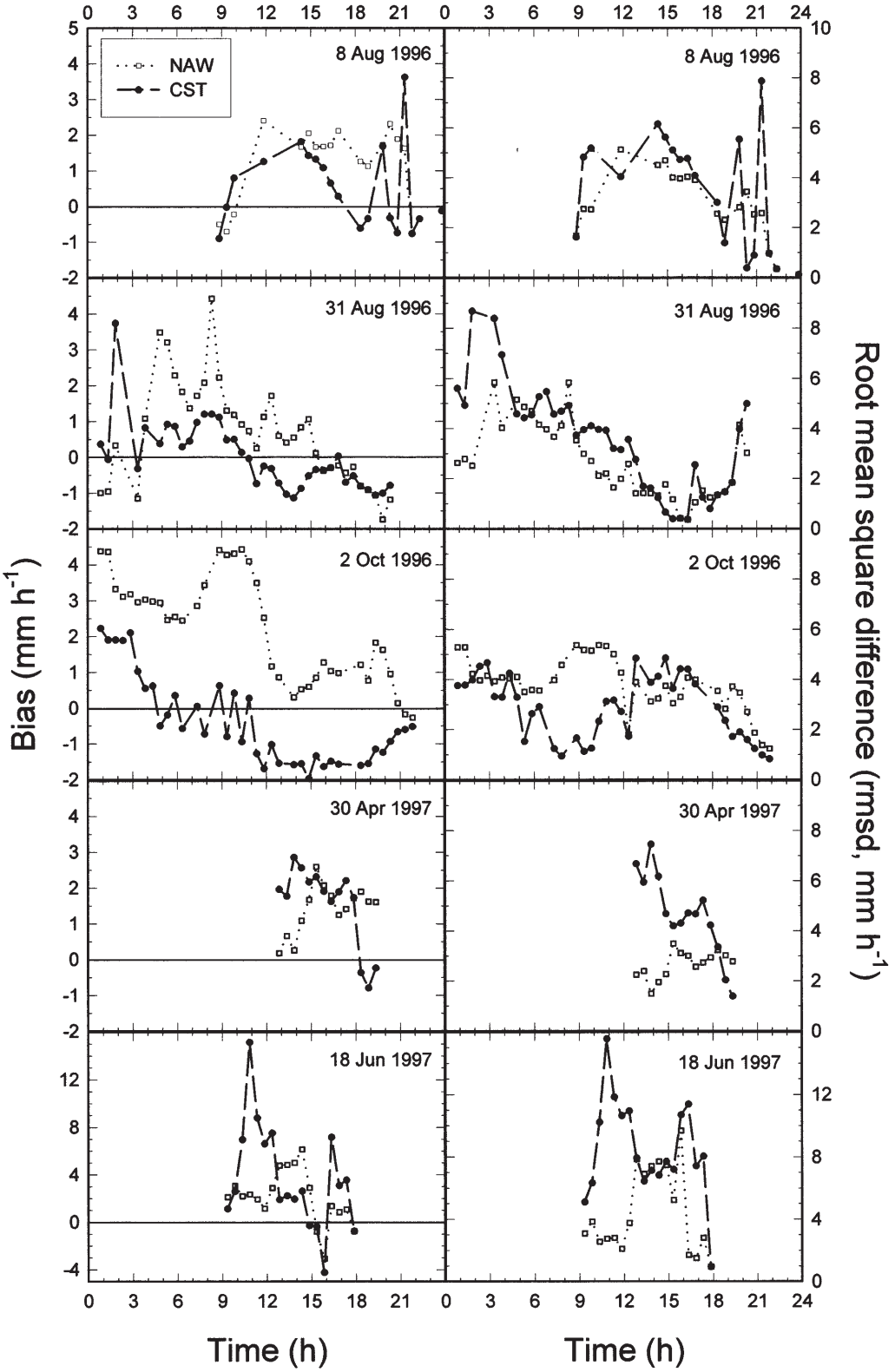

Figure 10. *Bias (left) and root mean square difference (rmsd) (right) in mm h^{-1} between radar rainrate and NAW (dotted + hollow square) and CST (dashed + filled circle).*

of CST in the morning, while in the afternoon it does not detect rain at all.

On 30 April 1997 both NAW and CST overestimate, NAW during the entire event while CST again drops to zero in the final part as shown also by the bias curves.

On 18 June 1997 both satellite estimations display two peaks. The first is caused by the presence of high, cold and stratified clouds eluding CST's cirrus screening and being classified as precipitating by NAW. Conversely the radar sees very little precipitation, determining the relatively high bias and rmsd values of the CST.

In all five cases NAW shows a tendency to significantly overestimate and CST to provide a better estimate of total rain despite the presence of pixels with great difference between radar-observed and CST-estimated rain, as shown by the high rmsd values.

The possibility of calibrating NAW into light rain (LR) and heavy rain (HR) classes for northern Italy convective activity was also explored for each image using the radar-observed mean rainrate within each satellite class. Results are reported in Figure 11. On 8 August 1996 no clear separation exists between LR and HR before 1551 UTC: the estimated rainrates do not match the ones observed by the radar (see Figure 9). The radar RHI (not shown) delineates some distinct convection cores, with the stratiform anvil clouds forming a compact structure at higher levels. The satellite senses the upper-level system and assigns heavy rain where the radar was retrieving none of it. A direct consequence is the low mean value of the observed precipitation in the HR class. During the final part of the event the two curves are distinct; this indicates a generally better delineation of the two rain classes by NAW in phase with the radar retrieval. The same is true for the 31 August 1996 storm for the overall event where the rainrate observed by the radar within the HR class is always higher than that observed within the LR class. On 2 October 1996 (frontally embedded convection) NAW does not discriminate between heavy and light rain, as demonstrated by the complete lack of separation between HR and LR curves. HR and LR are reasonably well separated during the first part of the 30 April 1997 isolated convective storm, when the storm was in its active build-up. When the anvil formed and convection started weakening, a clear-cut separation is no longer found. No firm conclusions can be drawn on the 18 June 1997 supercells. There are several possible reasons for this result.

(a) The supercells were embedded in a frontal system and the cold cloud area is then very much overestimated for the majority of the IR images, with no unique identification of convective cores.
(b) The supercell structure is normally tilted in the vertical so that the correspondence of upper-level temperature minima and low-level precipitation distribution is very risky.
(c) C-band weather radars are generally affected by attenuation (Doviak & Zrnic, 1993), which can be very significant for supercell storms (Holt *et al.*, 1997) till a complete extinction of the backscattering signal.

This latter obviously induces substantial underestimation of the rainfall amount: in the present case a rain-gauge 50 km from the radar in the attenuation area collected 20 mm in one hour, while the radar estimated 2.5 mm over the same period.

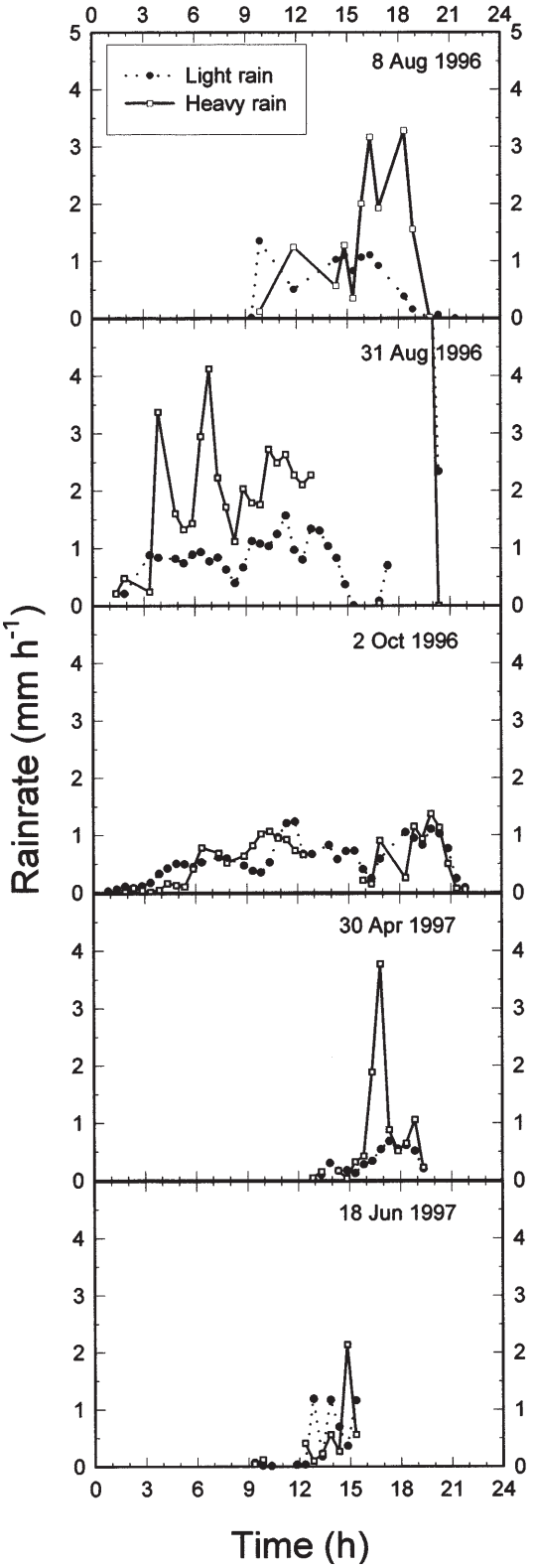

Figure 11. *Radar rainrate in mm h^{-1} within NAW's light rain (dotted + filled circle) and heavy rain (solid + hollow square) classes.*

6. WV-IR positive brightness temperature differences

Simultaneous observations of deep convective clouds in the infrared window region and the water vapour

absorption band (Schmetz *et al.*, 1997; Tjemkes *et al.*, 1997) have revealed that the equivalent brightness temperature in the latter is higher than in the former. The higher brightness temperature in the water vapour band (T_{WV}) than in the IR window (T_{IR}) is caused by the presence of water vapour in the stratosphere above the cloud (Fritz & Laszlo, 1993). This absorbs radiation from the cold cloud top and emits at stratospheric temperatures, normally higher than those at the top of the troposphere. Moreover, the amount of stratospheric water vapour and the location of the cloud top with respect to the tropopause are important parameters influencing the temperature difference.

Ackerman (1996) conducted a global analysis of the distribution of positive brightness temperature differences. Kurino (1997) used the two brightness temperature differences between the 11 and 12 μm and 11 and 6.7 μm channels of the Japanese Geostationary Meteorological Satellite (GMS) as independent variables for his empirical rainfall estimation algorithm. The former was used as a tool for the removal of thin non-precipitating cirrus (Inoue, 1987) and the latter as a parameter for the delineation of deep convection areas associated to heavy precipitation. No quantitative use of the water vapour band for satellite rainfall estimation is known at present.

The brightness temperature difference $\Delta T = T_{WV} - T_{IR}$ was computed for each pixel in the radar range and analysed against radar rainfall retrievals and satellite estimations. The pixels with $\Delta T > 0$ at 0951 UTC, 31 August 1996 are shown in Figure 12 emerging from the background of the METEOSAT IR image. Their distribution delimits the area of deep convection as in Schmetz *et al.* (1997) and Tjemkes *et al.* (1997).

The number of pixels with $\Delta T > 0$ (hereafter *NDT*) for each satellite scan is plotted together with the total radar-derived rainrate within the radar range in Figure 13. A general correspondence between *NDT* and rainrate exists for all five events, confirming the relationship between development of rain-bearing deep convective cells and the water vapour structure aloft. Interesting details emerge from a closer analysis of the maxima of *NDT* with respect to the highest rainrate. The 8 August 1996 maximum *NDT* is at 1551 UTC, whereas the maximum rainrate is at 1621 UTC, half an hour later. On 31 August 1996 *NDT* peaks at 0951 UTC and the rainrate has a distributed maximum between 0921 and 1121 UTC. The highest *NDT* is between 0951 and 1051 UTC on 2 October 1996, while the maximum rainrate is at 1121 UTC. On 30 April 1997 maxima of *NDT* and rainrate are reached between 1651 and 1751 UTC for the former and at 1721 UTC with a secondary maximum 1821 UTC for the latter. The highest *NDT* at 1351 UTC and highest rainrate at 1451 with a secondary peak at 1421 UTC characterise the 18 June 1997 supercells. The maximum *NDT* is always contemporary with the maximum observed rainrate, with a tendency to show up ahead of it of the order of half an hour.

The general tendency is confirmed by Figure 14, where *NDT* is superimposed on the number of rainy pixels as estimated by NAW and CST. For all cases, except 2 October 1996, which is not purely convective, the highest *NDT* values are in phase with maximum number of rainy pixels. CST assigns rain when $\Delta T > 0$, while NAW seems to be less dependent on *NDT*. This is attributable to the different physical principles of the two estimation methods. NAW rainfall is strictly related to the cold cloud top area, which maintains its relevance to the very last phases of the storm when the

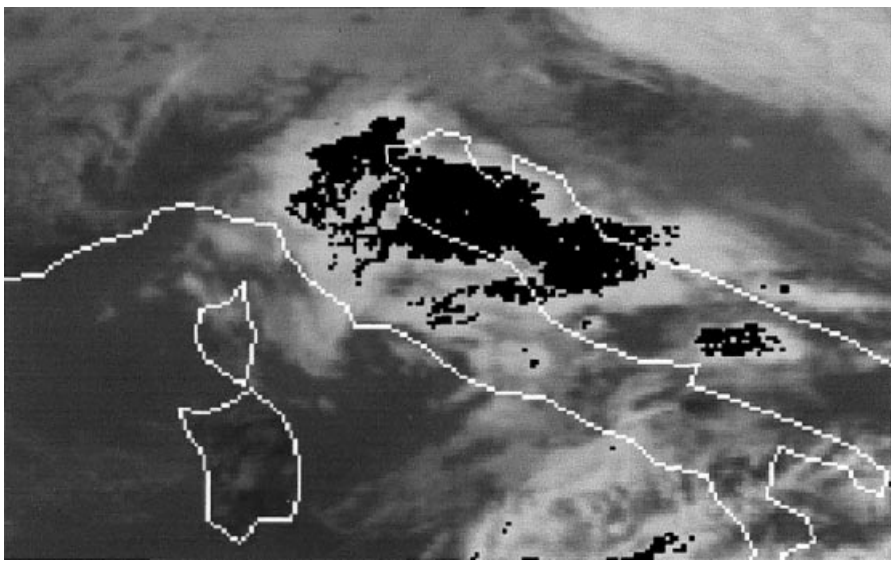

Figure 12. *METEOSAT infrared image at 0951 UTC on 31 August 1996. In black are the pixels corresponding to positive brightness temperature differences between water vapour and infrared channels.*

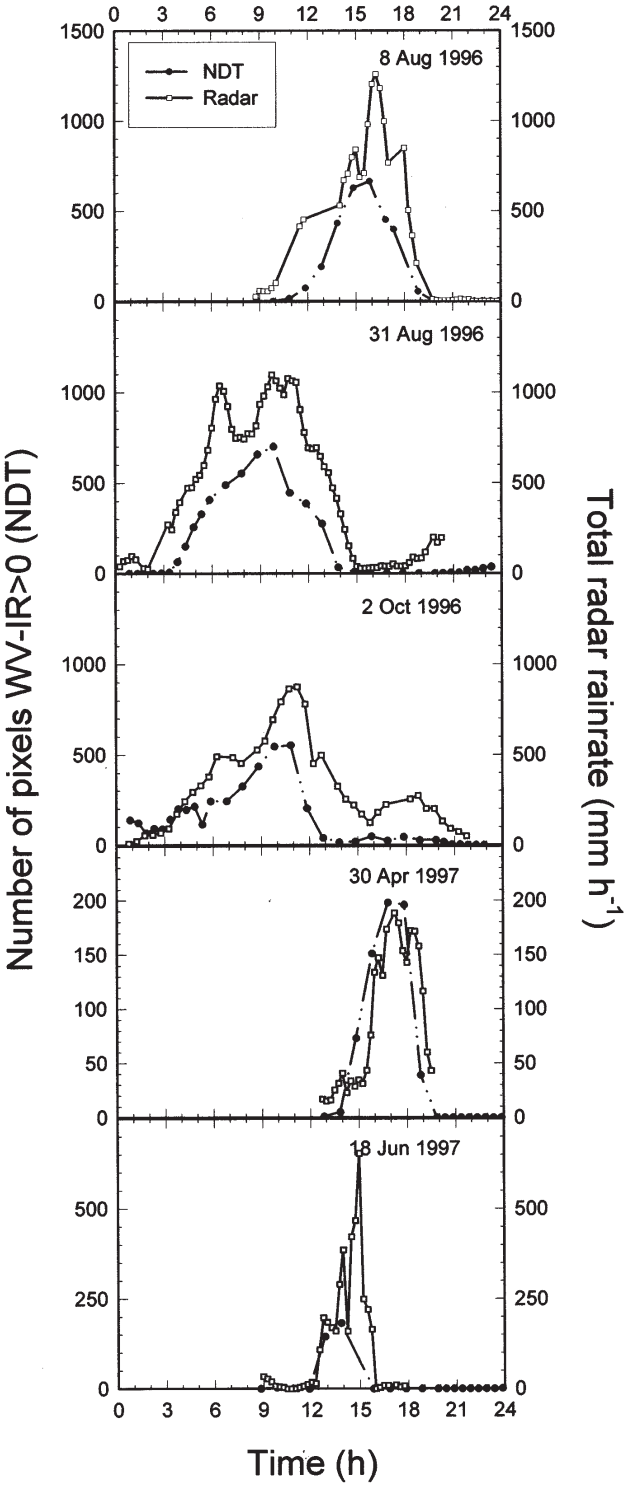

Figure 13. *Number of pixels corresponding to positive brightness temperature differences between water vapour and infrared channels over the radar coverage (dotted and filled circle) and total radar rainrate in mm h^{-1} (solid and hollow square). The former refers to the left axis and the latter to the right.*

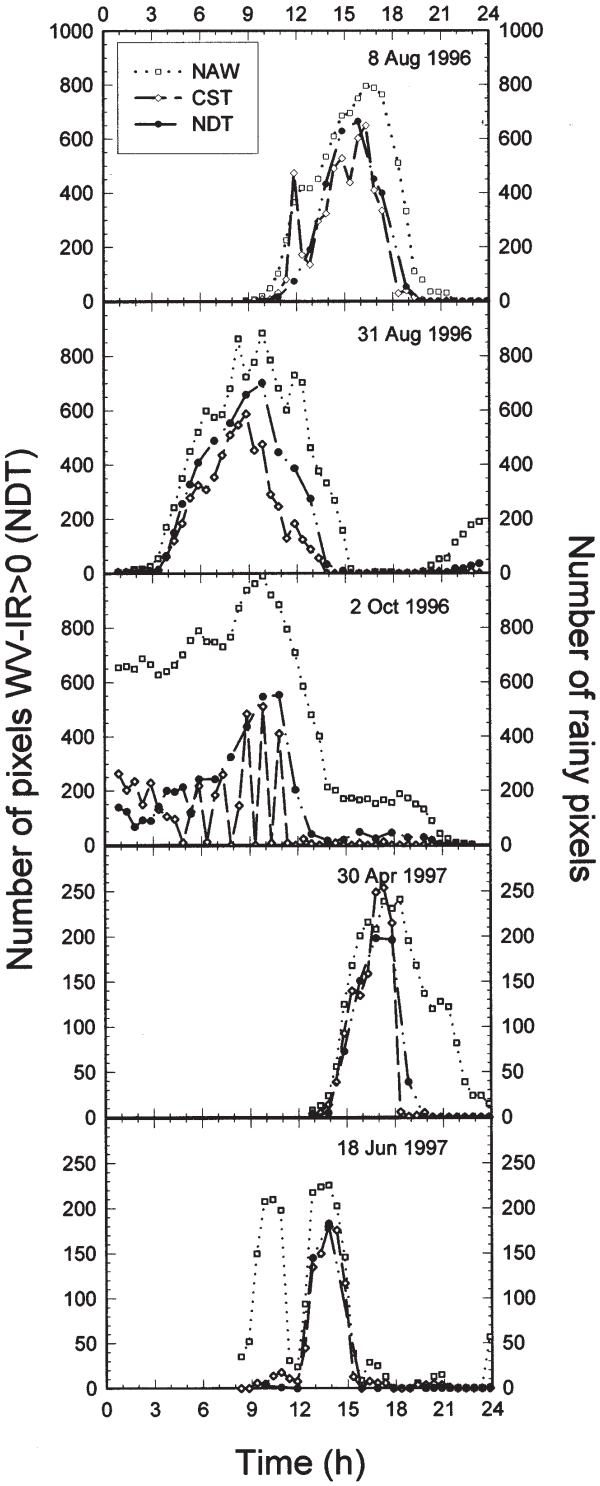

Figure 14. *Number of pixels corresponding to positive brightness temperature differences between water vapour and infrared channels over the radar coverage (solid and filled circle), number of rainy pixels as estimated by NAW (dotted and hollow square), and CST (dashed and hollow diamond).*

anvil has formed. The CST, on the other hand, assigns precipitation as a function of temperature minima, being more influenced by the initial stages of development characterised by the ascent of the air masses with a high water vapour content. At this time high cumulonimbus clouds reach the tropopause and the satellite senses areas with $\Delta T > 0$. This confirms once more the CST underestimation towards the end of the storm convective development, as previously noted.

7. Discussion

Rainfall from five convective episodes over northern Italy's Po Valley was estimated using METEOSAT's IR window channel and C-band weather radar data. The case studies are representative of the following categories: (a) spring isolated storm (30 April 1996), (b) early summer supercell (18 June 1997), (c) mid-summer convection (8 and 31 August 1996), and (d) early autumn embedded frontal convection (2 October 1996). Cacciamani *et al.* (1995) in their climatological study of thunderstorm activity over the Po Valley have shown that types (b) and (c) are the most frequent episodes, while almost the same number of significant events is found during the other two periods of the year. Present results are representative of the rainfall outcome under the above four mean convective conditions.

The contingency table analysis conducted using *CSI* and *FAR* parameters demonstrated that both satellite rainfall estimation techniques, NAW and CST, were reasonably effective in delimiting the rain areas. NAW is conceptually much simpler than CST, but its performances in setting the rain/no-rain limit were better. This is understandable since the method is based upon the delimitation of cold cloud top area instead of the computation of CST's temperature minima. The best results were obtained in the very central part of each convective event, when convective activity was growing and no signs of decay of the system were detected. The statistical parameters lost their significance at the beginning and the end of the storms, when the methods came across too few rainy pixels. The use of NAW for the satellite monitoring of convective rainfall areas is then conceivable given the limitations described above and already pointed out by, among others, Levizzani *et al.* (1990).

CST estimation is generally lower than the corresponding NAW estimate and closer to the radar retrieval. The examination of bias and rmsd between satellite-estimated and radar-observed rainrate showed a constant relatively lower bias of CST with respect to NAW. CST's rmsd, though, was frequently very similar to NAW's or even higher, discouraging one from considering bias an absolute indication of better CST performance.

Some very prominent peaks (e.g. 0821 UTC on 31 August 1996; see Figure 10) in the NAW rainrate and corresponding statistical parameters were found to be an artefact of the cold cloud top area assignment of the method. A large area around the convective system needs to be cut in order to avoid cutting out part of the cloud with the consequent wrong attribution of the coldest 50% and 10% coldest portions. While this is a positive precaution to be always taken when using NAW, it may sometimes reveal a problem when cold cirrus clouds from the anvil of one system reach out and overlap the cloud mass of a neighbouring storm. The cloud systems were in fact completely separated in the image of the previous scan but are considered 'connected' by the rain estimate for the present scan. This may significantly alter the rain assignment and induce spurious peaks not justified by the convective development.

NAW confirmed its tendency to an overall overestimation of rainfall given its lack of discrimination against cold non-precipitating cirrus and stratiform clouds in general. This becomes a very serious problem, especially for convection embedded in a frontal stratiform cloud background. The 2 October 1996 case closely resembles similar cases studied by Levizzani *et al.* (1990) or Porcù *et al.* (1996). CST results for such cases are also problematic, showing the jagged behaviour typical of a wrong rain detection mechanism. The technique does not identify the temperature minima required to assign convective rain because of the uniform frontal, low-temperature background.

The possibility of calibrating NAW into light rain and heavy rain classes by means of radar rainfall measurements was explored for all five cases. Results showed that a clear-cut separation between the two classes exists only for large convective summer storms that more closely resemble the tropical storms for which the technique was originally conceived.

The analysis of the correspondence of rainy pixels and rainrate with positive WV–IR brightness temperature differences *NDT* demonstrated the strict relationship between this parameter and the development of deep convective storms as shown by Schmetz *et al.* (1997) and Tjemkes *et al.* (1997). The use of *NDT* for qualitative monitoring of convective precipitation seems feasible, though more quantitative applications are far from being trivial. As for the IR channel, the WV band information content also belongs to the upper levels of the storm, making it difficult to find a one-to-one relationship with rainfall amount near the ground.

8. Conclusions

Given the above considerations, some conclusions can be drawn from the present study regarding the physics behind satellite rainfall estimation methods and their use for meteorological monitoring and nowcasting in particular.

The use of satellite IR data from geosynchronous spacecraft is still of great importance for rainfall monitoring, flash flood warning, numerical modelling, and operational hydrology. Pure IR techniques are also still used in operational configuration, though they require calibration by independent instruments. Vicente *et al.* (1998) use the IR channels of the Geostationary Operational Environmental Satellite (GOES-8/9) to compute real-time precipitation amounts based on a

power law algorithm. The regression is derived from a statistical analysis between surface instantaneous radar rainfall estimates and satellite IR cloud top temperatures collocated in time and space. The method is experimental and will soon be adopted as the operational method for the GOES satellite series. A radar network is necessary and the radar calibration needs to be checked very carefully. The method seems to be applicable chiefly to flash flood and other massive rainfall events.

Adler *et al.* (1993) have already carried out a comparison of IR rainfall estimates and low-orbit microwave (MW) retrievals from the Special Sensor Microwave/Imager (SSM/I), recognising the need for a more precise physical retrieval ensured by the microwave with respect to the IR cloud top inference. Their focus was, however, on monthly rainfall means far from the very rapid update cycle necessary to monitor deep convective storms. Levizzani *et al.* (1996) carried out a comparative study using IR and MW for two large convective storms over northern Italy. They found that the possibility existed for a calibration of more frequent but less precise estimations from the geostationary IR channels by less frequent but more physical retrievals from the MW. A combined MW + IR algorithm was presented by Vicente & Anderson (1994) for half-hourly estimates. One of the most up-to-date and sophisticated algorithms is that by Turk *et al.* (1998): its novelty is the use of near-real-time SSM/I data processed within two hours of the satellite orbit completion time. The synergy between geostationary IR and polar MW data for a close monitoring of convective rainfall appears to be the winning strategy given the current technological limitations in designing an MW sensor for geostationary orbit. Statistical approaches like that of Turk *et al.* (1998) ensure the best possible tuning of IR estimates.

The launch of METEOSAT Second Generation (MSG) scheduled for the year 2000 with the new Scanning Enhanced Visible and Infrared Radiometer (SEVIRI) (Woick *et al.*, 1996; Schmetz *et al.*, 1998) will make available 12 channels in the VIS, IR and near-IR, and ultraviolet (UV). The use of additional IR and near-IR channels for a multispectral rainfall estimation strategy has long been considered an interesting development (e.g. Vicente, 1996; Ba & Gruber, 1997) and will be very appealing with the new sensor. Moreover, the 15-minute scanning repetition time will further enable the development of the capability to monitor deep convection from the geostationary orbit. Convective rainfall rate products are currently under investigation (Fernandez *et al.*, 1998).

All currently available methods were mainly designed to account for young, vigorous convective clouds, mostly tropical, which are generally too violent in their overturning of the atmosphere to produce stratiform precipitation. In regions of older convection, however, the vertical motions are weaker, with particles growing by vapour diffusion, and the radar echoes are stratiform (Houze, 1997). The present study demonstrates that present satellite IR methods perform quite poorly at this stage of development of convection. The use of MW data is thought to be of some help since the MW signal is directly linked to the microphysics of the cloud. Radar calibration is another unavoidable step.

Other more sophisticated approaches are still very much experimental and concentrated at present in the Tropics like the Tropical Rainfall Measuring Mission (TRMM) (Kummerow *et al.*, 1998). In the long run the TRMM strategy of coupling VIS, IR, passive MW, precipitation radar, Earth radiation budget, and lightning detection on the same satellite platform will probably be the winning one.

In summary the results of the present study reveal all the capabilities and limitations of the pure IR rainfall estimation techniques and point towards the use of more complex methods.

(a) Using IR plus MW should give a better physical description of the structure of deep convection, resulting in better rainfall output from cloud top temperature data.
(b) The multispectral approach is not expected to add significant input on the microphysics of the cloud's interior but rather to give more information about the structure of the cloud top for a better rain area attribution.
(c) Use of radar networks and humidity model outputs for correlating rainfall rate and cloud top temperature fields.

Acknowledgements

The work was supported by: Consiglio Nazionale delle Ricerche (CNR), *Progetto Strategico MAP* and *Accordo CNR-CONICET*; Agenzia Spaziale Italiana (ASI); Agenzia Regionale Prevenzione e Ambiente (ARPA Emilia-Romagna)-Servizio Meteorologico Regionale, contract CR9701; the European Union through contract ENV4-CT96-0261. EUMETSAT support is gratefully acknowledged. Two anonymous reviewers provided helpful suggestions for the improvement of the paper.

References

Ackerman, S. (1996). Global satellite observations of negative brightness temperature differences between 11 and 6.7 μm. *J. Atmos. Sci.*, **53:** 2803–2812.

Adler, R. F. & Negri, A. J. (1988). A satellite infrared technique to estimate tropical convective and stratiform rainfall. *J. Appl. Meteorol.,* **27:** 30–51.

Adler, R. F., Negri, A. J., Keehn, P. R. & Hakkarinen, I. M. (1993). Estimation of monthly rainfall over Japan and sur-

rounding waters from a combination of low-orbit microwave and geosynchronous IR data. *J. Appl. Meteorol*., **32:** 335–356.

Alberoni, P. P., Buzzi, A. & Cacciamani, C. (1993). The episode of thunderstorm outbreak of 10 June 1990 over northern Italy. *Il Nuovo Cimento*, **16C:** 375–391.

Alberoni, P. P. & Nanni, S. (1996). Preliminary results of an anomalous propagation echoes suppression technique. *Proc. RADME96 Symp.: Theoretical, Experimental and Operational Aspects of Radarmeteorology*, 255–261.

Alberoni, P. P., Nanni, S., Crespi, M. & Monai, M. (1996). The supercell thunderstorm on 8 June 1990: mesoscale analysis and radar observations. *Meteorol. Atmos. Phys*., **58:** 123–138.

Alberoni, P. P., Costa, S., Nanni, S., Mezzasalma, P. & Levizzani, V. (1998). Analysis of two companion supercells over northern Italy. *Proc. COST-75 Advanced Weather Radar Systems Int. Seminar*, Locarno, Switzerland, 375–384.

Andersson, T., Alberoni, P. P., Mezzasalma, P., Michelson, D. B. & Nanni, S. (1997). Anomalous propagation identification from terrain and sea waves using vertical reflectivity profile analysis. *Prepr. 28th Conf. Radar Meteorology*, AMS, 93–94.

Arkin, P. A. (1979). The relationship between fractional coverage of high cloud and rainfall accumu-lations during GATE over the B-scale array. *Mon. Wea. Rev*., **106:** 1153–1171.

Arkin, P. A. & Meisner, B. N. (1987). The relationship between large-scale convective rainfall and cold cloud over the western hemisphere during 1982–84. *Mon. Wea. Rev*., **115:** 51–74.

Ba, M. B. & Gruber, A. (1997). Satellite retrieval of rainfall by the synergistic use of the solar reflected irradiance (3.9 µm) and brightness temperature (11 µm) as derived from GOES-8. *Proc. The 1997 Meteorological Satellite Data Users' Conf.*, EUMETSAT, 245–252.

Barrett, E. C. & Martin, D. W. (1981). *The Use of Satellite Data in Rainfall Monitoring*. Academic Press, 340 pp.

Barrett, E. C. & Michell, J. (1991). Satellite remote sensing of natural hazards and disasters in the Mediterranean. In *Current Topics in Remote Sensing*, **2**, ed. By E. C. Barrett, K. A. Brown and A. Michallef, Gordon & Breach, 51–67.

Bellon, A., Lovejoy, S. & Austin, G. L. (1980). Combining satellite and radar data for the short-range forecasting of precipitation. *Mon. Wea. Rev.*, **108:** 1554–1556.

Bendix, J. (1997). Adjustment of the convective stratiform technique (CST) to estimate 1991/93 El Niño rainfall distribution in Ecuador and Peru by means of Meteosat-3 IR data. *Int. J. Remote Sens.,* **18:** 1387–1394.

Buzzi, A. & Alberoni, P. P. (1992). Analysis and numerical modelling of a frontal passage associated with thunderstorm development over the Po Valley and the Adriatic Sea. *Meteorol. Atmos. Phys*., **48:** 205–224.

Cacciamani, C., Battaglia, F., Patruno, P., Pomi, L., Selvini, A. & Tibaldi, S. (1995). A climatological study of thunderstorm activity in the Po Valley. *Theor. Appl. Climatol*., **50:** 185–203.

Cheng, M. & Brown, R. (1995). Delineation of precipitation areas by correlation of METEOSAT visible and infrared data with radar data. *Mon. Wea. Rev.*, **123:** 2743–2757.

Doviak, R. J. & Zrnic, D. S. (1993). *Doppler Radar and Weather Observations*. 2nd edn, Academic Press, 562 pp.

Fernández, J. M., Legléau, H., Zwatz-Meise, V. & Dybbroe, A. (1998). The Satellite Application Facility (SAF) of EUMETSAT to support nowcasting: an introduction. *Prepr. 9th Conf. Satellite Meteorology Oceanography*, AMS, 319–322.

Fritz, S. & Laszlo, I. (1993). Detection of water vapor in the stratosphere over very high clouds in the tropics. *J. Geophys. Res*., **98 D12:** 22959–22967.

Griffith, C. G., Woodley, W. L., Grube, P. G., Martin, D. W., Stout, J. & Sikdar, D. N. (1978). Rain estimation from geosynchronous satellite imagery – visible and infrared studies. *Mon. Wea. Rev.*, **108:** 1153–1171.

Groginsky, H. L. & Glover, K. M. (1980). Weather radar canceller design. *Prepr. 19th Conf. Radar Meteorology*, AMS.

Gruber, A. (1973). Estimating rainfall in regions of active convection. *J. Appl. Meteorol.*, **12:** 110–118.

Holt, A. R., Watson, R. J., Chandra, M., Nanni, S. & Alberoni, P. P. (1997). A comparison of C-band observations using different polarization schemes. *Prepr. 28th Conf. Radar Meteorology*, AMS, 15–16.

Houze, R. A. Jr. (1997). Stratiform precipitation in regions of convection: a meteorological paradox? *Bull. Am. Meteorol. Soc.*, **78:** 2179–2196.

Inoue, T. (1987). A cloud type classification with NOAA 7 split-window measurements. *J. Geophys. Res.*, **92**: 3991–4000.

Kidder, S. Q. & Vonder Haar, T. H. (1995). *Satellite Meteorology: An Introduction*. Academic Press, 466 pp.

Kummerow, C., Barnes, W., Kozu, T., Shiue, J. & Simpson, J. (1998). The Tropical Rainfall Measuring Mission (TRMM) sensor package. *J. Atmos. Oceanic Technol*., **15:** 809–817.

Kurino, T. (1997). A satellite infrared technique for estimating 'deep/shallow' convective and stratiform precipitation. *Adv. Space Res*., **19:** 511–514.

Levizzani, V. (1998). Intense rainfall monitoring from geostationary satellites. *Prepr. 9th Conf. Satellite Meteorology Oceanography*, AMS, 327–330.

Levizzani, V., Porcù, F. & Prodi, F. (1990). Operational rainfall estimation using METEOSAT infrared imagery: an application in Italy's Arno River basin – its potential and drawbacks. *ESA J.*, **14:** 313–323.

Levizzani, V., Porcù, F., Marzano, F. S., Mugnai, A., Smith, E. A. & Prodi, F. (1996). Investigating a SSM/I microwave algorithm to calibrate METEOSAT infrared instantaneous rainrate estimates. *Meteorol. Appl*., **3:** 5–17.

Levizzani, V., Amorati, R., Alberoni, P. P., Nanni, S. & Rizzi, R. (1997). Satellite and radar analysis of convective precipitation in northern Italy: a cloud structure point of view. *Proc. The 1997 Meteorological Satellite Data Users' Conf.*, EUMETSAT, 285–292.

Levizzani,V., Alberoni, P. P., Amorati, R., Masuelli, S., Costa, S., Holmlund, K., Schmetz, J. & Tjemkes, S. A. (1998). Severe weather on 18 June 1997: A MAP supercell case study. *MAP Newsletter*, 9, 16–17.

Marrocu, M., Pompei, A., Dalu, G., Liberti, G. L. & Negri, A. J. (1993). Precipitation estimation over Sardinia from satellite infrared data. *Int. J. Remote Sens.*, **14:** 115–134.

Marshall, J. S. & Palmer, W. M. K. (1948). The distribution of rain drops with size. *J. Meteorol*., **5**, 165–166.

Negri, A. J., Adler, R. F. & Wetzel, P. J. (1984). Rain estimation from satellite: an examination of the Griffith–Woodley technique. *J. Climate Appl. Meteorol.*, **23:** 102–116.

Negri, A. J. & Adler, R. F. (1993). An intercomparison of three satellite infrared rainfall techniques over Japan and surrounding waters. *J. Appl. Meteorol.,* **32:** 357–373.

Petty, G. W. (1995). The status of satellite-based rainfall estimation over land. *Remote Sens. Environ*., **51:** 125–137.

Pompei, A., Marrocu, M., Boi, P. & Dalu, G. (1995). Validation of retrieval algorithms for the infrared remote sensing of precipitation with the Sardinian rain gauge network data. *Il Nuovo Cimento*, **18C:** 483–496.

Porcù, F., Borga, M. & Prodi, F. (1996). Precipitation fields analysis: case studies using satellite, radar and raingauges network. *Proc. The 1996 Meteorol. Satellite Data Users' Conf.*, EUMETSAT, 313–320.

Porcù, F., Borga, M. & Prodi, F. (1998). A radar-satellite rainfall estimation technique for hydrological applications. *Prepr. 9th Conf. Satellite Meteorology and Oceanography*, AMS, 287–290.

Prodi, F. (1974). Combined photo and radar observations of storms in the Po Valley. *Riv. It. di Geofisica*, **XXIII:** 82–88.

Prodi, F. & Wirth, E. (1973). Mesoscale and microphysical investigation of an isolated hailstorm. *Riv. It. di Geofisica*, **XXII:** 165–185.

Schmetz, J., Tjemkes, S. A., Gube, M. & van de Berg, L. (1997). Monitoring deep convection and convective overshooting with METEOSAT. *Adv. Space Res.*, **19:** 433–441.

Schmetz, J., Woick, H., Tjemkes, S. A. & Rattenborg, M. (1998). From METEOSAT to METEOSAT Second Generation (MSG). *Prepr. 9th Conf. Satellite Meteorology and Oceanography*, AMS, 335–338.

Scofield, R. A. & Naimeng, L. (1994). The use of satellite imagery during the great floods of 1993. *Prepr. 7th Conf Satellite Meteorology and Oceanography*, AMS, 345–350.

Tjemkes, S. A., van de Berg, L. & Schmetz, J. (1997). Warm water vapour pixels over high clouds as observed by METEOSAT. *Beitr. Phys. Atmosph.*, **70:** 15–21.

Todd, M. C., Barrett, E. C., Beaumont, M. J. & Green, J. L. (1995). Satellite identification of rain days over the upper Nile River basin using an optimum infrared rain/no-rain threshold temperature model. *J. Appl. Meteorol.*, **34:** 2600–2611.

Tsonis, A. A. & Isaac, G. A. (1985). On a new approach for instantaneous rain area delineation in the midlatitudes using GOES data. *J. Clim. Appl. Meteorol.*, **24:** 1208–1218.

Turk, F. J., Marzano, F. S. & Smith, E. A. (1998). Combining geostationary and SSM/I data for rapid rain rate estimation and accumulation. *Prepr. 9th Conf. Satellite Meteorology and Oceanography*, AMS, 462–465.

Vicente, G. A. (1996). Algorithm for rainfall rate estimation using a combination of GOES-8 11.0 and 3.9 micron measurements. *Prepr. 8th Conf. Satellite Meteorology Oceanography*, AMS, 274–278.

Vicente, G. A. & Anderson, J. R. (1994). A new rain retrieval technique that combines geosynchronous IR and MW polar orbit data for hourly rainfall estimates. *Prepr. 7th Conf. Satellite Meteorology Oceanography*, AMS, 34–37.

Vicente, G. A. & Scofield, R. A. (1996). Experimental GOES-8/9 derived rainfall estimates for flash flood and hydrological applications. *Proc. The 1996 Meteorol. Satellite Data Users' Conf.*, EUMETSAT, 89–96.

Vicente, G. A., Scofield, R. A. & Menzel, W. P. (1998). The operational GOES infrared rainfall estimation technique. *Bull. Am. Meteorol. Soc.*, **79:** 1883–1898.

Wilks, D. S. (1995). *Statistical Methods in the Atmospheric Sciences*. Academic Press, 467 pp.

Woick, H., Schmetz, J. & Tjemkes, S. A. (1997). An introduction to METEOSAT Second Generation imagery and products. *Proc. The 1997 EUMETSAT Meteorological Satellite Data Users' Meeting*, 395–400.